SCIENCE CHINA
Technological Sciences

October 2010 Vol.53 No.10: 2792–2807
doi: 10.1007/s11431-010-4087-0

Optimization design study of low-Reynolds-number high-lift airfoils for the high-efficiency propeller of low-dynamic vehicles in stratosphere

MA Rong[1*], ZHONG BoWen[2] & LIU PeiQing[1]

[1] *Key Laboratory of Fluid Mechanics, Ministry of Education, Institute of Fluid Mechanics, School of Aeronautical Science and Engineering, Beijing University of Aeronautics and Astronautics, Beijing 100191, China;*
[2] *Department of Aerospace Science, School of Engineering, Cranfield University, MK43 0AL, United Kingdom*

Received March 20, 2009; accepted June 28, 2009

Aerodynamic performance of low-Reynolds-number high-lift airfoil makes a great impact on designing a high-efficiency propeller for low-dynamic vehicles in stratosphere. At high altitude, low-Reynolds-number airfoils are supposed to have high lift-drag ratio or high endurance factor at cruising attack angle along with good stall characteristics. To design such a high-performance low-Reynolds-number high-lift airfoil, the paper established a hierarchical multi-objective optimization platform by combing direct search optimization algorithm EXTREM and airfoil flow field solver XFOIL to automatically and quickly calculate aerodynamic performance function of airfoil by computer. It provides an effective solution to multi-point design problem of low-speed low-Reynolds-number airfoil. It can be seen from the results of three typical optimization examples, the new airfoil E387_OPT2, FX63-137_OPT2 and S1223_OPT2 based on hot low-Reynolds-number high-lift airfoils (Eppler 387 airfoil, Wortmann FX63-137 airfoil and S1223 airfoil) can meet the optimization design requirements and have very good aerodynamic characteristics in both design state and non-design state. Thus, the applicability and effectiveness of hierarchical multi-objective optimization platform are verified.

multi-objective optimization, low Reynolds number airfoil, EXTREM, hierarchical multi-objective optimization

Citation: Ma R, Zhong B W, Liu P Q. Optimization design study of low-Reynolds-number high-lift airfoils for the high-efficiency propeller of low-dynamic vehicles in stratosphere. Sci China Tech Sci, 2010, 53: 2792–2807, doi: 10.1007/s11431-010-4087-0

Along with the development of high technology in aeronautics, astronautics and materials, and the surge in oil prices caused by the world-wide oil crisis, a new hot research focus arises in the aircraft family members—low-dynamic vehicles in stratosphere. The flight velocity and acceleration of a low-dynamic vehicle are small; flight posture and path are invariant in time in stratosphere (at the height of 10 to 50 km above the ground, which is between the highest flight height of aircraft and the lowest height of the satellite orbit). It can be divided into the airship and the long-endurance UAVs. When the low-dynamic vehicle flies in stratosphere, it shows the advantages of long endurance and the functions of large transport aircraft, so it is widely used in the place of military surveillance, communications support and anti-submarine warfare [1], as shown in Figure 1 [2]. It can be known from the advanced design of the high-altitude UAVs (predators I/II, Helios, Pathfinder, etc.) and high-altitude airships (British Skyship500/600 and the United States A30, 80, 130 etc.), the propulsion system for the advanced low-dynamic vehicles is generally a high-power DC motor-driven propeller system [3, 4], as shown in Figure 2. The propeller which can turn the engine momentum into the thrust has become a preferred propulsion system for low

*Corresponding author (email: rong.jessica@hotmail.com)

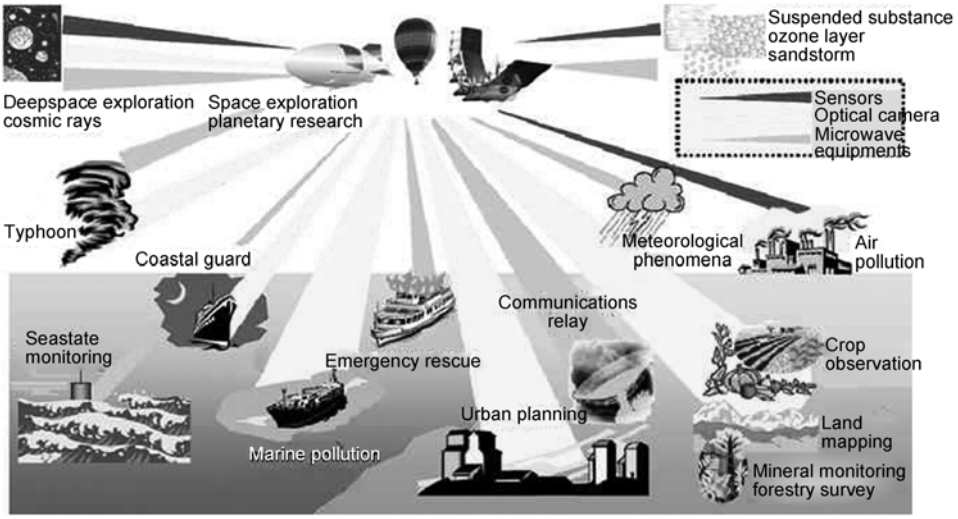

Figure 1 High altitude information platform.

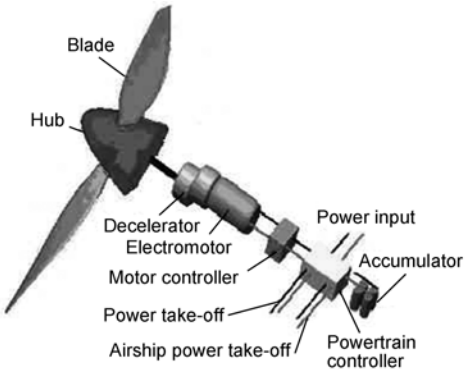

Figure 2 Propeller system composition.

dynamic aircrafts in stratosphere, because of the advantages in economic and security. In order to make full use of the power of engine or electromotor and reduce the energy consumption, the propeller system needs improving efficiency and reducing weight as far as possible. Therefore, it is very important to develop a high efficiency propeller adaped to a large span of flight height and the low-density atmospheric environment in stratosphere, which can reduce energy demand and flight load, promote the overall design, reduce cost and gain great social and economic benefits in the current situation of energy shortage and severe environmental problems. What is more, it also brings a new challenge for the traditional propeller design and manufacturing technology.

Airfoil performance has a decisive impact on the propeller aerodynamic performance. Compared with aerodynamic parameters at low altitude, there are great differences when an aircraft operates in stratosphere, such as the smaller atmospheric density, lower air pressure, larger air kinematic viscosity coefficient, smaller speed of sound, etc. This makes the range of Reynolds number of the propeller airfoils under study fall between 10^5 and 10^6, which belongs to low Reynolds number. In the low Reynolds number condition, the aerodynamic characteristics of an airfoil shows some new characteristics, such as the rapidly descending maximum lift-to-drag ratio of common airfoils [5] and the non-linear phenomena of symmetrical airfoils at small attack angles, especially near 0° [6, 7], etc. A lot of researches showed that the above phenomena are closely related with the laminar flow separation phenomenon [8], as shown in Figure 3 [9]. For subsonic flows, the laminar boundary layer over an airfoil at a low Reynolds number has been observed to separate and

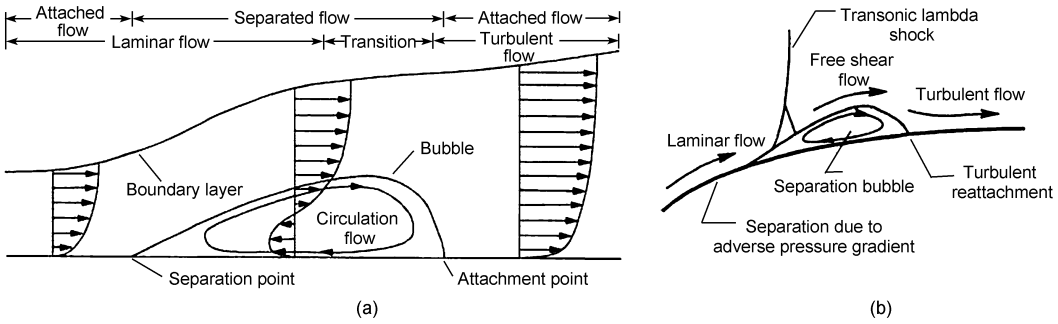

Figure 3 Boundary layer schematic diagram on the upper surface of low Reynolds number airfoil. (a) Low Mach number; (b) high Mach number.

reattach to the airfoil surface to form a laminar separation bubble even at small attack angles, which would decrease the efficiency of propeller sharply and reduce aerodynamic performance of the propeller dramatically.

Therefore, one of the challenges to propeller designers for low-dynamic vehicles in stratosphere is to design high-performance low-speed low-Reynolds-number airfoils. A great deal of existing data reveals [10] that instead of using current existing airfoils, many aircrafts have utilized special airfoils which are more adequate to their functional requirements. For the low-dynamic vehicles at high altitude, the requirements are listed as follows:

1) High operational lift coefficient C_l;

2) High lift-to-drag ratio C_l/C_d;

3) High endurance factor $C_l^{1.5}/C_d$;

4) High maximum lift coefficient $C_{l\max}$;

5) Very mild stall characteristics for enough safety margins;

6) Limited pitching moment coefficient C_m;

7) Wide range of low resistance.

However, in the absence of experimental data of low Reynolds number, the means of wind tunnel tests to design a new airfoil is very difficult, which always needs a long period, a high cost and rich experience [11]. In recent years, computational fluid dynamics (CFD) becomes a kind of important design and calculation method and is used in the airfoil design and the flow field analysis more frequently [11]. In most cases, aerodynamic design methods based on CFD are divided into two types including inverse design and optimization design. The aerodynamic optimization design is a combination of aerodynamic analysis and optimization method, which achieves the best aerodynamic performance under given constraint conditions by changing the aerodynamic shape of design target by using the computer. Every constraint algorithm can be applied directly to the optimization process, while the constrained problem can also be conveniently converted to unconstrained problem. So the optimization design method brings more flexibility and use value.

In order to design a high-performance low-Reynolds-number high-lift airfoil which can adapt to low-density atmospheric environment in stratosphere, a hierarchical multi-objective optimization platform is established by combing direct search optimization algorithm EXTREM [12] with flow field solver XFOIL [13, 14]. The XFOIL is based on a panel method with compressibility correction for subsonic airfoils. The optimization method is coupled with XFOIL to achieve computer automatic optimization based on analytic function linear superposition method used for establishing the shape of airfoils, while the hierarchical multi-objective optimization method is adopted to consider the off-design performance as well. It provides an effective solution to multi-point design problem of low-speed low-Reynolds-number airfoil. The paper presents the multi-objective aerodynamic optimization and numerical solve process on the three hot low-Reynolds-number high-lift airfoils and discusses the three typical optimization examples. Thus, the applicability and effectiveness of the hierarchical multi-objective optimization platform are verified.

1 Design method

1.1 Airfoil shape parameterization method

As airfoil shape parameterization method has a direct impact on the results of airfoil optimization design, it could directly affect airfoil aerodynamic characteristics. There are many ways to describe airfoil shape such as polynomial fitting and analytic function linear superposition. This paper is using analytic function linear superposition method [15], which represents the new airfoil shape defined by the basic airfoil, the shape function and corresponding coefficients.

$$\begin{aligned} y_{\text{upper}}(x) &= y_{\text{ou}} + \sum_{k=1}^{N} c_k f_k(x), \\ y_{\text{lower}}(x) &= y_{\text{ol}} + \sum_{k=1}^{N} c_{k+7} f_k(x), \end{aligned} \tag{1}$$

where y_{ou} and y_{ol} are the ordinates of the upper and lower surfaces of the initial airfoil, N and c_k represent the number and coefficient of parameters, respectively which could control the airfoil shape. $f_k(x)$ represents the Hicks-Henne shape function [16].

$$f_k(x) = \begin{cases} x^{0.25}(1-x)e^{-20x}, & k=1, \\ \sin^3(\pi x^{e(k)}), & k>1, \end{cases} \tag{2}$$

where $e(k) = \dfrac{\log 0.5}{\log x_k}$. Here, x_k (k=1,2, $\cdots$,7) are 0.012, 0.15, 0.3, 0.45, 0.6, 0.75, 0.9 respectively.

1.2 Flow solver for subsonic airfoil

Drela's XFOIL uses a linear-vorticity panel method for inviscid analysis coupled with an integral boundary-layer method for viscous analysis. For the design and analysis of subsonic isolated airfoils, it has been evaluated by many designs [13]. The suitability of XFOIL for quick preliminary estimate of transition position has been demonstrated [13]. So in the optimization design process, XFOIL (version 6.94) is employed for the calculation of the airfoil aerodynamic characteristics at low-speed and low Reynolds numbers, and estimate the chord-wise location of transition from laminar to turbulent flow x_{tr} using an envelope e^n-type method. For the current work, a value of n_{crit} = 9 has been assumed for the critical transition amplification factor, which is typical for a smooth blade surface in a low-turbulence environment and all of the analyses have been conducted

using the free-transition option, in which the code computes the transition location as a part of the solution procedure. Each airfoil was represented in XFOIL using 230 panels distributed using XFOIL's default paneling routine.

1.3 Numerical optimization algorithm

Optimization algorithm is an important part in the aerodynamic shape optimization design system. The individual objective function in this paper is minimized by the direct search optimization algorithm EXTREM, which is developed by Jacob, because of its quick convergence and no derivation [12]. The EXTREM optimization algorithm is a direct search method which can be used effectively for solving the multi-variable constrained optimization problem without calculating the derivative of object function. The search direction is determined just the same as Rosenbrock's method. If it is a constrained optimization problem with N variables, the first main search direction is determined by the initial value $\boldsymbol{C}$ and the initial search step $\boldsymbol{DC}$ (manually input according to the requirements) in the following manner:

$$\boldsymbol{S} = \boldsymbol{C} + \boldsymbol{DC}. \tag{3}$$

By means of a Gram-Schmidt orthogonalization, N–1 secondary search directions are determined. After the search along every secondary search direction, the extremum of (k+1)th optimum is attained. The optimization process in one direction is implemented by a parabolic extrapolation, just like Powell's method:

$$\boldsymbol{C}_4 = \boldsymbol{C}_1 + \frac{\boldsymbol{DC}}{\left|F_3 - 2F_1 + F_2\right|} \times \frac{F_2 - F_3}{2 \times N}, \tag{4}$$

where the maximum is obtained when N=+1 and the minimum is obtained when $N = -1$.

The next main search direction, $\boldsymbol{S}^{(k+1)}$, always results from connecting the extremum of (k+1)th optimum $\overline{X}^{(k+1)}$ and the one of kth optimum $\overline{X}^{(k)}$:

$$\overline{S}^{(k+1)} = \overline{X}^{(k+1)} - \overline{X}^{(k)}. \tag{5}$$

All kinds of constraints can be taken into account, but the optimization variables in each search or extrapolation process must be checked whether they have violated the given constraints. If the variables have violated, they will be managed in the following two ways.

In the search process, if $\boldsymbol{C}_2 = \boldsymbol{C}_1 + \boldsymbol{DC}$ violates the given constraints, $\boldsymbol{C}_2$ will be changed to $\boldsymbol{C}_{2\text{new}} = \boldsymbol{C}_1 + \boldsymbol{DC}/2$.

In the extrapolation process, if $\boldsymbol{C}_4$ violates the given constraints, $\boldsymbol{C}_4$ will be changed to $\boldsymbol{C}_{4\text{new}} = \boldsymbol{C}_1 + (\boldsymbol{C}_4 - \boldsymbol{C}_1)/4$.

The method described above has been shown having quick convergence [12].

1.4 Hierarchical multi-objective optimization method

The typical form of mathematical model of the multi-objective optimization is as below.

$$\begin{cases} \min f_1(\boldsymbol{x}), \quad \boldsymbol{x} = \left[x_1, x_2, \cdots, x_n\right]^{\mathrm{T}} \in E^n, \\ \min f_2(\boldsymbol{x}), \\ \cdots \\ \min f_q(\boldsymbol{x}), \end{cases} \tag{6}$$

subject to: $g_i(\boldsymbol{x}) \leqslant 0,\ i = 1, 2, \cdots, m.$

In the multi-objective optimization design, it is difficult to make all sub-objectives optimal at the same time. It occurs often that the performance of one orsome sub-objectives turn worse as a result of one sub-objective minimization. That is to say, the optimizations among sub-objectives contradict each other in the process of minimizing. Therefore, it is necessary to coordinate and make some concession among the optimal values of the sub-objective functions $f_1(\boldsymbol{x}), f_2(\boldsymbol{x}), \cdots, f_q(\boldsymbol{x})$ in order to obtain a better overall optimal solution. In order to design a high-performance high-lift and low-Reynolds-number airfoil which can adapt to low-density atmospheric environment in stratosphere no matter in design condition or in off-design condition, the hierarchical multi-objective optimization method [17] is adopted as the multi-objective optimization method used in this paper.In the hierarchical multi-objective optimization method, objective functions are listed in order of importance. Every objective function is minimized:

$$\text{Minimize} \quad f_i(\boldsymbol{X}), \tag{7}$$

where i = 1, 2, $\cdots$, k. From i = 2 to i = k, $f_i(\boldsymbol{X}^{(k)})$ subject to:

$$f_{i-1}(\boldsymbol{X}^{(k)}) \leqslant \left(1 + \varepsilon_{j-1}/100\right) \times f_{i-1}(\boldsymbol{X}^{(k-1)}), \tag{8}$$

where j =2, 3, $\cdots$, i and ε_{j-1} is the given increment of (j–1)th objective function. So the optimum point $\boldsymbol{X}^{(k)}$ is finally obtained.

2 Flow solver verification

The accuracy of aerodynamic design and analysis method is an important factor to determine the quality of the optimization result, which decides the success or failure of the optimization design. Its results cannot be used with any confidence until calculated performance is in good agreement with the experimental data. So before the airfoil optimization is carried out, the accuracy and reliability of XFOIL will be validated by comparing the experimental data of Eppler 387 airfoil (Figure 4), at low Mach number and low Reynolds number, as shown in Figure 5.

Data taken on the E387 airfoil at low-speed and low-Reynolds-number are shown in Figure 5, compared with

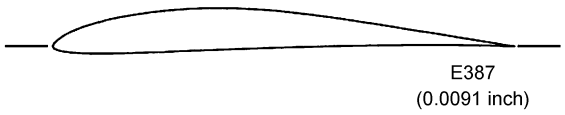

Figure 4 Contours of E387.

experiment data taken in a low-turbulence pressure tunnel [18–20]. As seen, good agreement is observed. To sum up, the results calculated by XFOIL at low speed and low Reynolds number have a good agreement with the experimental data.

3 Design examples and discussion

In various design problems, different constraints may be applied to the airfoil geometry depending on the specific requirements. For low Reynolds number airfoils, friction drag is the main one in airfoil drags, which is closely related to the transition position. Airfoils at low Reynolds numbers have low skin friction drag because of the inherent laminar boundary layer formation. The challenge in low Reynolds number airfoil optimization design is an optimization of transition position to maintain low airfoil drag. So it allows that both upper and lower surfaces vary in different manners in airfoil optimization design to get better aerodynamics characteristics and a suitable transition position.

3.1 Design case I—E387 airfoil optimization and analysis

Airfoils with high lift-to-drag ratios are suitable for low Reynolds number (Re_c <10^6) applications [21]. Eppler 387 airfoil is chosen as a basic airfoil in the optimization design case I.

The general design targets are as following:

1) The lift-drag ratio C_l/C_d in cruising condition α=3° can reach 130 with a lift coefficient higher than that of E387 which is 0.74;

2) Maximum-lift-coefficient $C_{l\max}$ at climbing attack angle α=12° is higher than that of E387 which is 1.277;

3) Wide range of low drag coefficient.

The design conditions of the low speed low-Reynolds-number airfoil for this investigation were chosen as Ma = 0.13, Re=0.46×10^6. In addition to providing a maximum lift-drag ratio C_l/C_d at design point, the optimized airfoil must satisfy certain maximum thickness constraint and has a good property of stall characteristics. So the optimized airfoil is supposed to have the maximum thickness and the leading edge radius unreduced (to avoid stall-incidence and $C_{l\max}$ decreasing) compared with E387 airfoil.

A. Single-objective optimization

The single design objective for the low-Reynolds-number airfoil E387 is to maximize the lift-drag ratio C_l/C_d on the design condition of Ma=0.13, Re=0.46×10^6 and α=3° with a limitation of lift coefficient higher than that of E387 which is 0.74. The optimized airfoil of the single-objective

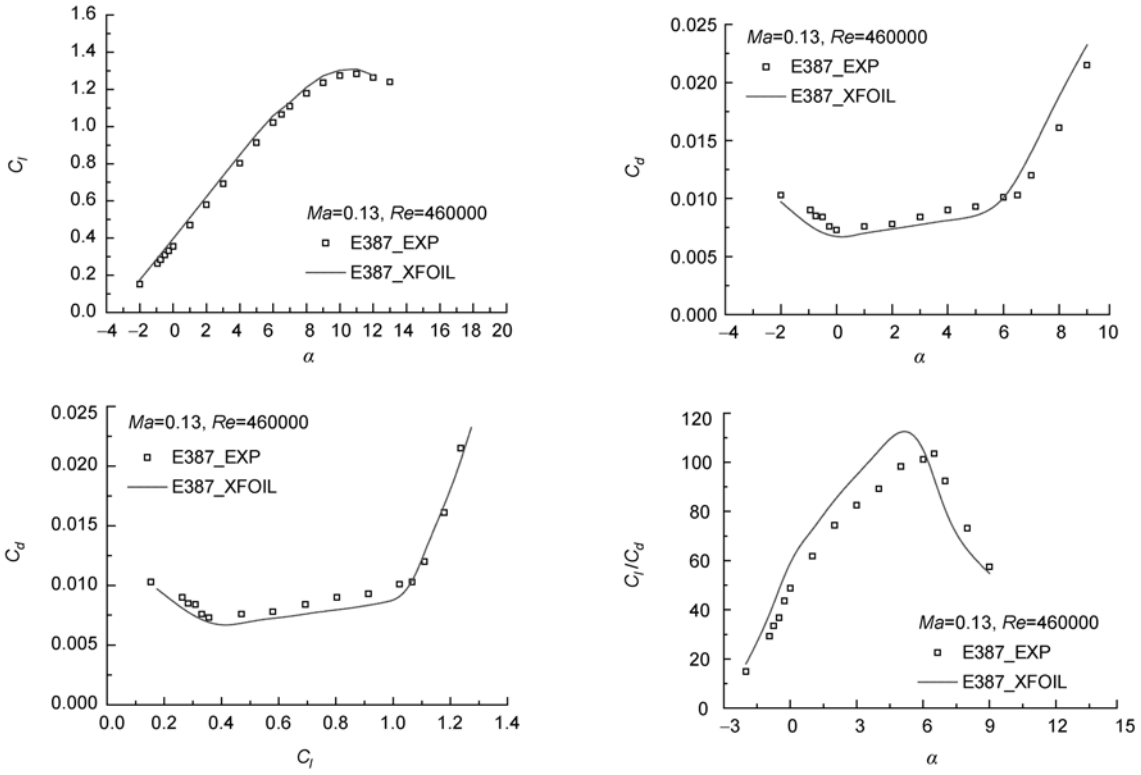

Figure 5 Aerodynamic data comparison between calculation and experiment of E387 at Ma = 0.13 and Re =0.46×10^6.

optimization is described as E387_OPT1 airfoil. Calculation data comparison between E387 and the optimized airfoil E387_OPT1 at the design attack angle α=3° are shown in Table 1, while the contour and surface static pressure distribution comparisons between E387 and E387_OPT1 are shown in Figures 6 and 7.

As shown in Figure 8, the aerodynamic character of E387_OPT1 is better than that of E387, which postpones the transition position on the supper surface of airfoil at the design attack angle α=3° and has moved downstream the

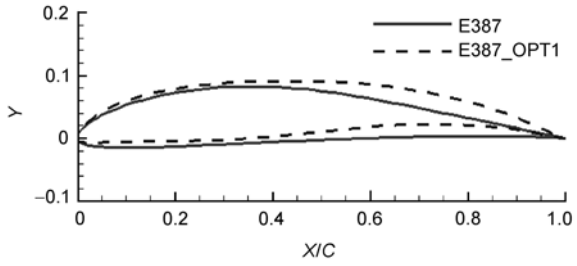

Figure 6 Contour comparison between E387 and E387_OPT1.

Table 1 Results comparison between E387 and E387_OPT1 at the design attack angle α=3°

	C_l	ΔC_l	C_d	ΔC_d	C_l/C_d	$\Delta(C_l/C_d)$
E387_EXP_3°	0.69		0.0084		82.1	
E387_XFOIL_3°	0.74		000776		94.9	
E387_OPT1_3°	1.05	42%	0.00718	–7.5%	146.2	54%

ΔC_l, ΔC_d and $\Delta(C_l/C_d)$ represent the change percentages of lift coefficient, drag coefficient, lift-drag ratio compared with E387 by XFOIL calculation.

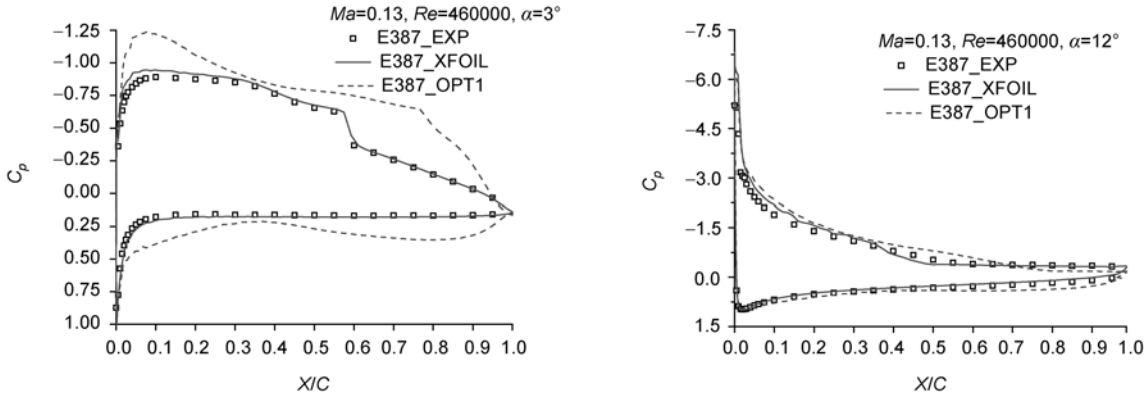

Figure 7 The surface static pressure distribution comparison between E387 and E387_OPT1.

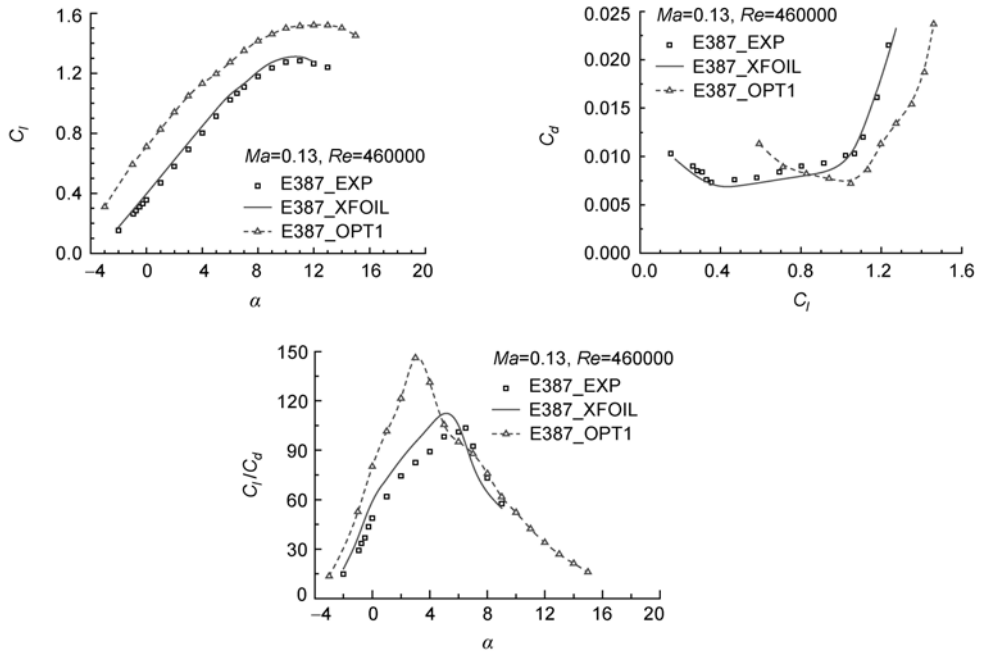

Figure 8 Comparison between experiment data, calculation data of E387 and calculation data of E387_OPT1.

separate location of upper surface at α=12° (the position of C_p restored to the largest pressure straight line is rearward), compared with E387 shown in Figure 7. The results calculation by XFOIL show that the entire lower surface of E387_OPT1 experiences laminar flow, while the transition position of the upper surface of E387_OPT1 changes from 57% chord of E387 to 77% chord at the design attack angle α=3°. The stall-incidence of E387_OPT1 computed by XFOIL is about 12°, an increase of 1°, compared with E387. The static pressure coefficient of optimized airfoil is steeper on the leading edge of the upper surface in order to resist stronger adverse pressure gradient and push the transition location further downstream. This pressure distribution of E387_OPT1 can increase effectively the stability of the boundary layer, allowing transition to occur later. From Table 1, the calculation results of XFOIL match the experimental data very well for E387. It can be seen clearly that E387_OPT1 has a good aerodynamic performance at the design attack angle α=3°, whose lift-drag ratio rises from 94.9 to 146.2, an increase of 54%, compared with E387. The lift coefficient increases 42% and the drag coefficient decreases 7.5%. The aerodynamic characteristics at α=12° has also been checked. From Figure 8, it can be seen that E387_OPT1 has a higher lift coefficient (reaching 1.522) compared with E387 airfoil (1.277), an increase of 19.2% has been achieved. So the optimization work for higher lift coefficient on the climbing condition doesn't need to conduct.

It is well known that the single-objective optimization can easily lead to a local extreme. This phenomenon can also be seen from Figure 8, in particular the lift-drag ratio plot. Although E387_OPT1 has good aerodynamic performance at the design angle α=3°, it performs badly at the off-design attack angles α=4°, 5°, 6°, due to the rapid increase in the drag. The airfoil is not suitable for practical use. Therefore, a multiple design-point multi-objective optimization has been conducted, whose results are presented below.

B. Multi-objective optimization

According to the hierarchical multi-objective optimization method, the primary objective function of bi-objective optimization design here (at the basis of E387_OPT1) is minC_d at the primary design attack angle α=6°, while the secondary objective function here is $(C_d/C_l)_{\mathrm{E387\_OPT2}} \leqslant 1.1\times(C_d/C_l)_{\mathrm{E387\_OPT1}}$ at the secondary design attack angle α=3°, subject to:

1) $(C_l)_{\mathrm{E387\_OPT2}} \geqslant (C_l)_{\mathrm{E387}}$ at the primary design attack angle α=6°;

2) $(C_l)_{\mathrm{E387\_OPT2}} \geqslant (C_l)_{\mathrm{E387}}$ at the secondary design attack angle α=3°;

3) $(C_d)_{\mathrm{E387\_OPT2}} \leqslant (C_d)_{\mathrm{E387}}$ at the secondary design attack angle α=3°.

The optimized airfoil of the multi-objective optimization is described as E387_OPT2 airfoil. Calculation data comparison between E387 and E387_OPT2 at the primary design attack angle α=6° and the secondary design attack angle α=3° are shown in Table 2. The comparisons of the contours and surface static pressure distributions among E387, E387_OPT1 and E387_OPT2 are shown in Figures 9 and 10.

Figure 11 presents that the aerodynamic character of E387_OPT2 is significantly better than those of E387 and E387_OPT1, which postpones the transition position on the supper surface of airfoil at α=6° and 3° and has moved downstream the separate locations at large attack angle α=12°, compared with E387, as shown in Figure 10. The calculation results of XFOIL show that the entire lower surface of E387_OPT2 experiences laminar flow, while the transition position of the upper surface of E387_OPT2 changes from 33% chord of E387 to 53% chord at the primary design attack angle α=6° and the transition position of the upper surface of E387_OPT2 changes from 57% chord of E387 to 67% chord at the secondary design attack angle α=3°. The stall-incidence of E387_OPT2 computed by XFOIL is up to 14°, an increase of 3°, compared with E387. From Table 2, it can be clearly seen that E387_OPT2

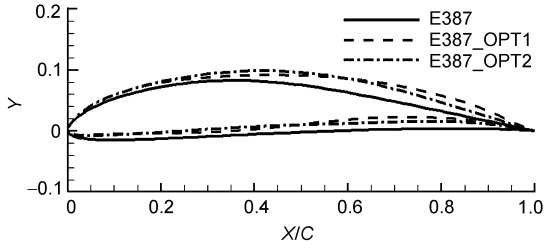

Figure 9 Contours among E387, E387_OPT1 and E387_OPT2.

Table 2 Results comparison between E387 and E387_OPT2 at multiple design-points

	C_l	ΔC_l	C_d	ΔC_d	C_l/C_d	$\Delta(C_l/C_d)$
E387_EXP_6°	1.022		0.0101		101.2	
E387_XFOIL_6°	1.06		0.010		105.0	
E387_OPT2_6°	1.3	22.6%	0.009	−10%	144.4	37.5%
E387_EXP_3°	0.693		0.0084		82.5	
E387_XFOIL_3°	0.74		0.0078		94.9	
E387_OPT2_3°	1.01	36.5%	0.00776	−0.5%	130	37%

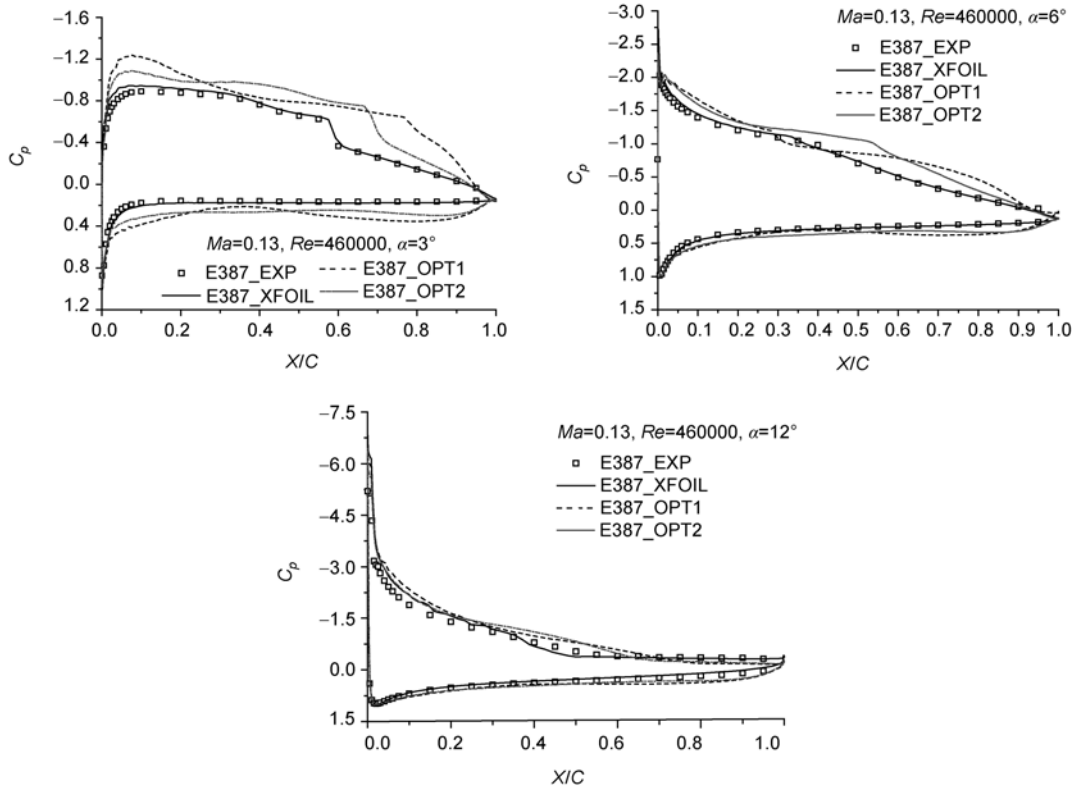

Figure 10 The surface static pressure distribution comparison among E387, E387_OPT1 and E387_OPT2.

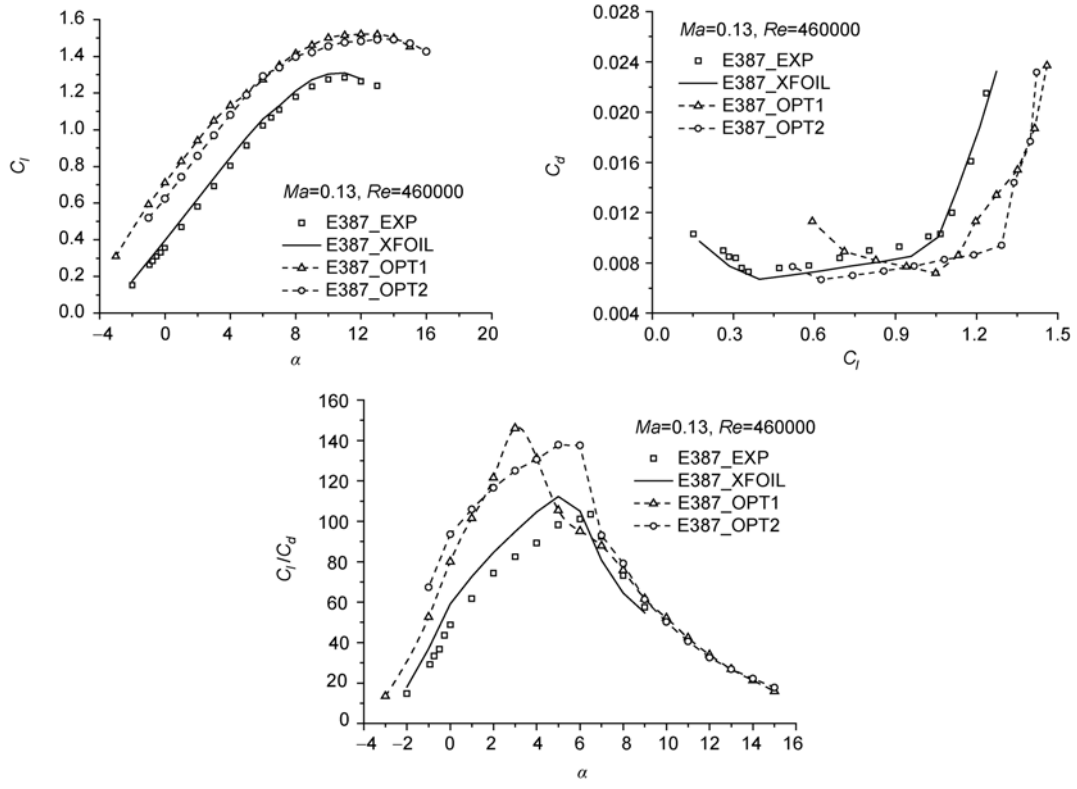

Figure 11 Comparison among experiment data, calculation data of E387 and calculation data of E387_OPT1 and E387_OPT2.

has a good aerodynamic performance at α=3° and 6°. The drag coefficient of E387_OPT2 declines from 0.01 to 0.009 at the primary design attack angle α=6°, a decrease of 10%, along with an increasing lift-coefficient of 22.6% (reaching 1.3), compared with E387, which is obviously better than E387_OPT1 at off-design attack angles α=4°, 5° and 6°. The lift-drag ratio rises from 94.9 to 130.0 at the secondary design attack angle α=3°, an increase of 37%, compared with E387, along with an increasing lift coefficient of 36.5% (reaching 1.01) and without the drag coefficient increase. At the same time, we can see that E387_OPT2 has satisfied the requirement of higher lift coefficient on the climbing attack angle α=12° as well, whose lift coefficient raises from 1.277 to 1.49, an increase of 16.7%, compared with E387, along with a wide range of low drag.

As will be readily seen, the multiple design-points multi-objective optimization example for E387 airfoil produces a satisfactory result.

3.2 Design case II—FX63-137 airfoil optimization and analysis

FX63-137 airfoil is chosen as the basic airfoil in the optimization design case II. Long-endurance has become one of the new targets in recent R&D activities for air-vehicles. Examples include the ERAST (Environmental Research and Sensor Technology) project of NASA, and other long-endurance airplane and methods investigations in the world [22]. Typical applications of such flights include communication relay, natural environmental protection, and disaster survey. The mission duration of these so-called "atmospheric satellites" varies from 20 to 100 h.

The general design targets are as follows:

1) The long-endurance factor $C_l^{1.5}/C_d$ in cruising condition α=3° can be 155 with a lift coefficient higher than that of FX63-137 which is 1.256;

2) High maximum-lift-coefficient $C_{l\max}$ at climbing attack angle α=13° can be larger than that of E387 which is 1.7;

3) Wide range of low drag.

The design conditions of the low-speed low-Reynolds-number airfoils for this investigation were chosen as Ma = 0.1, Re=0.5×10^6. In addition to greatly increasing the long-endurance factor $C_l^{1.5}/C_d$ at the design point, the optimized airfoil must satisfy certain maximum thickness constraint and has a good property of stall characteristic. So the optimized airfoil should have the maximum thickness and the leading edge radius unreduced compared with FX63-137.

A. Single-objective optimization

The single design-point of the low-Reynolds-number airfoil FX63-137 on the conditions of Ma=0.1 and Re= 0.5×10^6 is the maximum long-endurance factor $C_l^{1.5}/C_d$ at the design attack angle α=3° with a limitation of a lift coefficient higher than that of FX63-137 which is 1.256. The optimized airfoil of the single-objective optimization is described as FX63-137_ OPT1 airfoil. Calculation data comparison between FX63-137 and FX63-137_OPT1 at the design attack angle α=3° are shown in Table 3, while the contour and surface static pressure distribution comparisons between FX63-137 and FX63-137_OPT1 are shown in Figures 12 and 13.

As shown in Figure 14, the lift characteristic of FX63-137_OPT1 is better than that of FX63-137, which postpones the transition position on the supper surface of airfoil at the design attack angle α=3° and has moved downstream the separate location of upper surface at α=13°, compared with FX63-137, as shown in Figure 13. The results calculation by XFOIL show that the entire lower surface of FX63-137_OPT1 experiences laminar flow, while the transition position of the upper surface of FX63-137_ OPT1 changes from 53.1% chord of FX63-137 to 65.7% chord at the design attack angle α=3°. From Table 3, it can be seen clearly that FX63-137_OPT1 has a good aerodynamic performance at the design attack angle α=3°, whose long-endurance factor raises from 134.5 to 156.4, an increase of 16.3%, compared with FX63-137, along with lift coefficient 3.6% increase (reaching 1.3) and drag coefficient decrease 9.5% (reaching 0.0095). At the same time, it is obviously seen in Figure 14 that FX63-137_OPT1 has satisfied a requirement of higher lift coefficient on the climbing attack angle α=13° as well, whose lift coefficient raises from 1.7 to 1.79, an increase of 5.3%, compared with FX63-137.

But it also can be seen that FX63-137_OPT1 also has a bad performance at the off-design attack angles (less than α=0°) from the drag character and the long-endurance factor character, as plotted in Figure 14, which is not suitable for practical use. So the work of multi-objective optimization needs to conduct, which is presented below.

B. Multi-objective optimization

According to the hierarchical multi-objective optimization method, the bi-objective optimization design proceeded at the basis of FX63-137_OPT1, whose primary objective function here is minC_d at the primary design attack angle α=−1°, while the secondary objective function here is $\left(C_d/C_l^{1.5}\right)_{\text{FX63-137\_OPT2}} \leqslant 1.08\times\left(C_d/C_l^{1.5}\right)_{\text{FX63-137\_OPT1}}$ at the

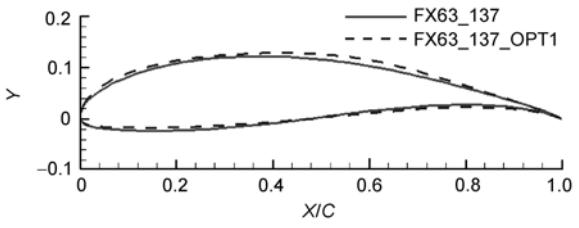

Figure 12 Contour comparison between FX63-137 and FX63-137_OPT1.

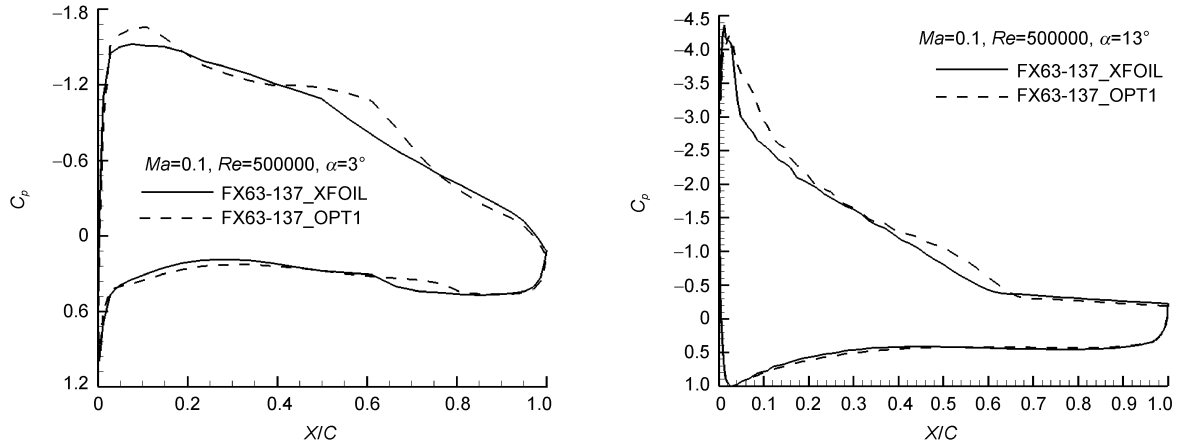

Figure 13 The surface static pressure distribution comparison between FX63-137 and FX63-137_OPT1.

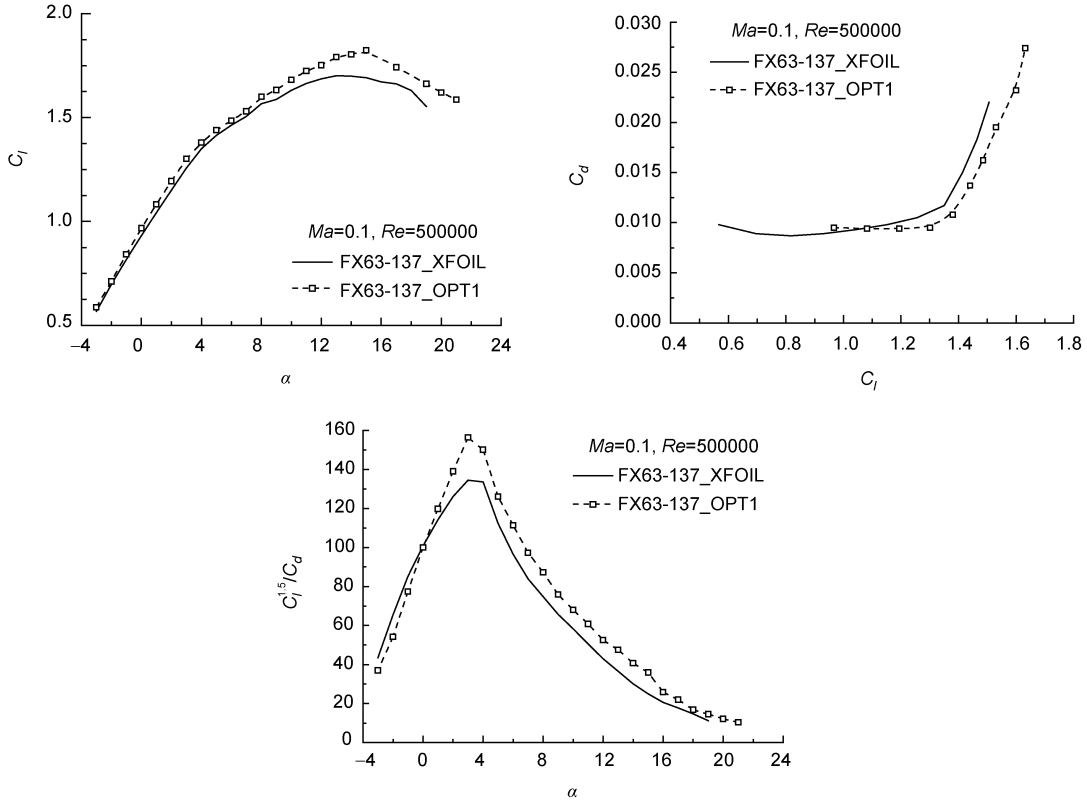

Figure 14 Calculation data comparison between FX63-137 and FX63-137_OPT1.

Table 3 Results comparison between FX63-137 and FX63-137_OPT1 at α=13° and 3°

	C_l	ΔC_l	C_d	ΔC_d	$C_l^{1.5}/C_d$	$\Delta(C_l^{1.5}/C_d)$
FX63_137_XFOIL_3°	1.256		0.0105		134.5	
FX63_137_OPT1_3°	1.301	3.6%	0.0095	–9.5%	156.4	16.3%
FX63_137_XFOIL_13°	1.7014		0.0607		36.5	
FX63_137_OPT1_13°	1.791	5.3%	0.0504	–17%	42.6	16.7%

secondary design attack angle α=3°, subject to:

1) $(C_l)_{\text{FX63-137\_OPT2}} \geqslant (C_l)_{\text{FX63-137}}$ at the primary design attack angle α=−1°;

2) $(C_l)_{\text{FX63-137\_OPT2}} \geqslant (C_l)_{\text{FX63-137}}$ at the secondary design attack angle α=3°;

3) $(C_d)_{\text{FX63-137\_OPT2}} \leqslant (C_d)_{\text{FX63-137}}$ at the secondary design attack angle α=3°.

FX63-137_OPT2 airfoil represents the optimized airfoil

of the multi-objective optimization at the basis of FX63-137_OPT1 airfoil. The calculation data comparison between FX63-137 and FX63-137_OPT2 at the primary design attack angles $\alpha=-1°$ and the secondary design attack angle $\alpha=3°$ are shown in Table 4. Figures 15 and 16 show the comparisons of the contours and surface static pressure distributions among FX63-137, FX63-137_OPT1 and FX63-137_OPT2.

The aerodynamic character of FX63-137_OPT2 is significantly better than those of FX63-137 and FX63-137_OPT1 as shown in Figure 17, which postpones the transition position on the supper surface of airfoil at small attack angle $\alpha=3°$ and has moved downstream the separate locations at large attack angle $\alpha=13°$ compared with FX63-137, as shown in Figure 16. The calculation results of XFOIL show that the entire lower surface of FX63-137_OPT2 experiences laminar flow, while the transition position of the upper surface of FX63-137_OPT2 changes from 69.5% chord of FX63-137 to 79.2% chord at the primary design attack angle $\alpha=-1°$, and the transition position of the upper surface of FX63-137_OPT2 changes from 53.1% chord of FX63-137 to 63.4% chord at the secondary design attack angle $\alpha=3°$. The stall-incidence of FX63-137_OPT2 computed by XFOIL is up to 16°, an increase of 3°, compared with FX63-137. In Table 4, it can be clearly seen that FX63-137_OPT2 optimized by the bi-objective optimization has a perfect performance at $\alpha=-1°$, 3°, and 13°. The drag coefficient of FX63-137_OPT2 decreases about 1% at the primary design attack angle $\alpha=-1°$ as compared with FX63-137, which is better than the FX63-137_OPT1 at the off-design attack angles (less than $\alpha=0°$). The long-endurance factor rises from 134.5 to 157.2 at the secondary design attack angle $\alpha=3°$, an increase of 16.9%, compared with FX63-137, along with lift coefficient 10.3% increase (reaching 1.385) and without drag coefficient increase. It also can be seen that FX63-137_OPT2 satisfies the requirement of a higher maximum lift coefficient on the climbing attack angle $\alpha=13°$ as well, whose lift coefficient raises from 1.7 to 1.8, an increase of 5.8%, as compared with FX63-137.

So the multiple design-points multi-objective optimization example for FX63-137 airfoil produces a satisfactory result.

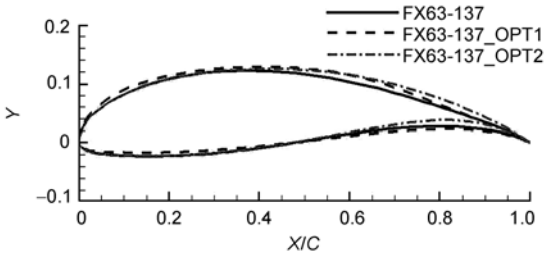

Figure 15 Contour comparison among FX63-137, FX63-137_OPT1 and FX63-137_OPT2.

Table 4 Results comparison between FX63-137 and FX63-137_OPT2 at multiple design-points

	C_l	ΔC_l	C_d	ΔC_d	$C_l^{1.5}/C_d$	$\Delta(C_l^{1.5}/C_d)$
FX63_137_XFOIL_–1°	0.8176		0.0087		85.2	
FX63_137_OPT2_–1°	0.973	19%	0.0086	–1.2%	111.3	30.6%
FX63_137_XFOIL_3°	1.256		0.0105		134.5	
FX63_137_OPT2_3°	1.385	10.3%	0.0104	–1%	157.2	16.9%
FX63_137_XFOIL_13°	1.7014		0.0607		36.5	
FX63_137_OPT2_13°	1.80	5.8%	0.0569	–6.3%	42.4	16.2%

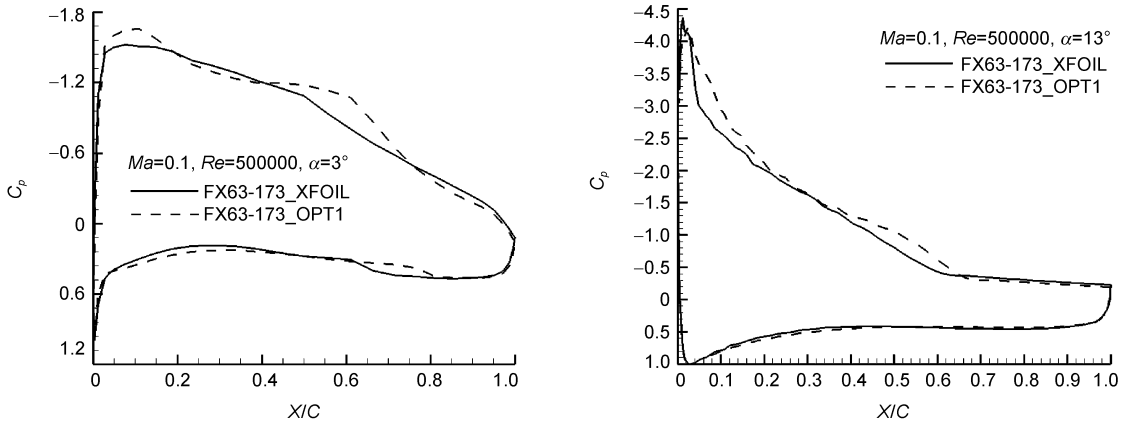

Figure 16 The surface static pressure distribution comparison among FX63-137, FX63-137_OPT1 and FX63-137_OPT2.

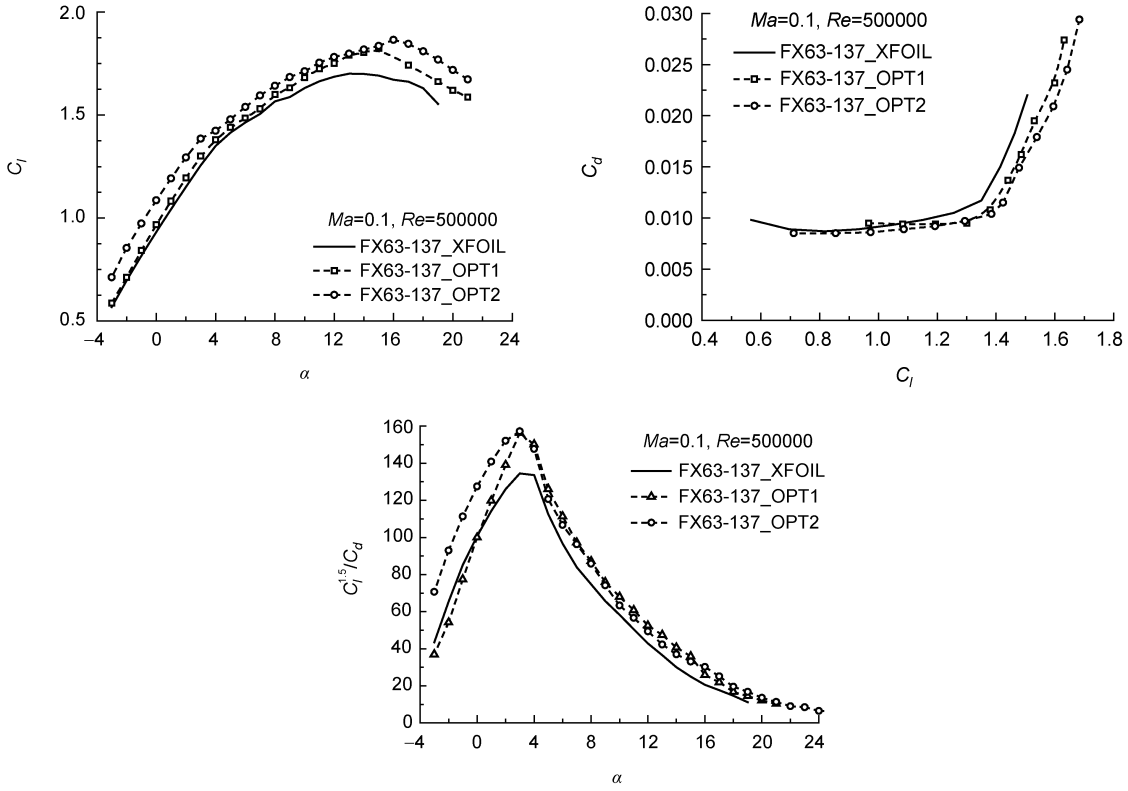

Figure 17 Calculation data comparison among FX63-137, FX63-137_OPT1 and FX63-137_OPT2.

3.3 Design case III—S1223 airfoil optimization and analysis

From ref. [22], it shows that the S1223 has high $C_{l\max}$, nearly a 25% increase compared with the FX 63-137. This characteristic is important for some UAVs that operate with the airfoil near $C_{l\max}$ to achieve low-speed flight requirements for loiter, cruise, or landing. What is more, the S1223 exhibits acceptable moderate stall characteristics much like the M06-13-128. From the above mentioned, the S1223 has the aerodynamic advantages of both the FX63-137 and the M06-13-138. High lift is rarely the only desirable feature of an airfoil. From ref. [22], it presents that the S1223 has larger drag at the same time, which need improving in order to get high lift-drag ratio. So the S1223 is chosen finally as the initial airfoil for optimization design case III.

The general design targets are as following:

The drag-coefficient C_d in cruising condition α=3° can reach 0.0145 with a lift coefficient higher than that of S1223 which is 1.49;

Lift-coefficient C_l at climbing attack angle α=12° is higher than that of S1223 which is 2.20;

Wide range of low drag coefficient.

The design conditions of the low-Reynolds-number airfoil for this investigation were chosen as Ma=0.1, Re=0.5×10^6. In addition to providing a minimum drag-coefficient C_d at design point, the optimized airfoil must satisfy certain maximum thickness constraint and has a good property of stall characteristics. So the optimized airfoil is also supposed to have the maximum thickness and the leading edge radius unreduced (to avoid stall-incidence and $C_{l\max}$ decreasing) compared with S1223 airfoil.

A. Single-objective optimization

The single design objective for the low-Reynolds-number airfoil S1223 is to minimize the drag-coefficient C_d on the design condition of Ma=0.1, Re=0.5×10^6 and α=3° with a limitation of lift coefficient higher than that of S1223 which is 1.49. The optimized airfoil of the single-objective optimization is described as S1223_OPT1 airfoil. Calculation data comparison between S1223 and the optimized airfoil S1223_OPT1 at the design attack angle α=3° are shown in Table 5, while the contour and surface static pressure distribution comparisons between S1223 and S1223_OPT1 are shown in Figures 18 and 19.

As shown in Figure 20, the aerodynamic character of S1223_OPT1 is better than that of S1223. From Table 5, it can be seen clearly that E387_OPT1 has a good aerodynamic performance at the design attack angle α=3°, whose drag-coefficient reduce from 0.016 to 0.0125, an decrease of 21.9%, compared with S1223. The lift coefficient increases 8.34% and the lift-drag ratio increases 32.3%. While the aerodynamic characteristics at $\alpha \geqslant 12°$ are bad with smaller lift-efficient and larger drag-coefficient, compared with S1223. So the multi-optimization work for keeping

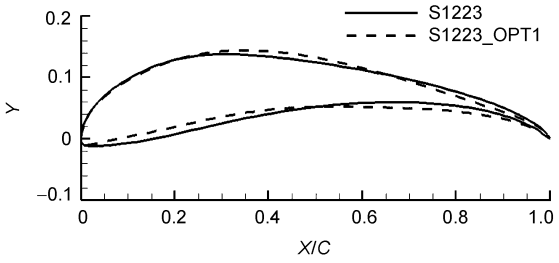

Figure 18 Contour comparison between S1223 and S1223_OPT1.

high lift-coefficient at $\alpha \geqslant 12°$ need to conduct.

B. Multi-objective optimization

According to the hierarchical multi-objective optimization method, the primary objective function of bi-objective optimization design here (at the basis of S1223_ OPT1) is $\max(C_l)$ at the primary design attack angle $\alpha=12°$, while the secondary objective function here is $(C_d)_{\text{S1223\_OPT2}} \leqslant 1.1\times(C_d)_{\text{S1223\_OPT1}}$ at the secondary design attack angle $\alpha=3°$, subject to:

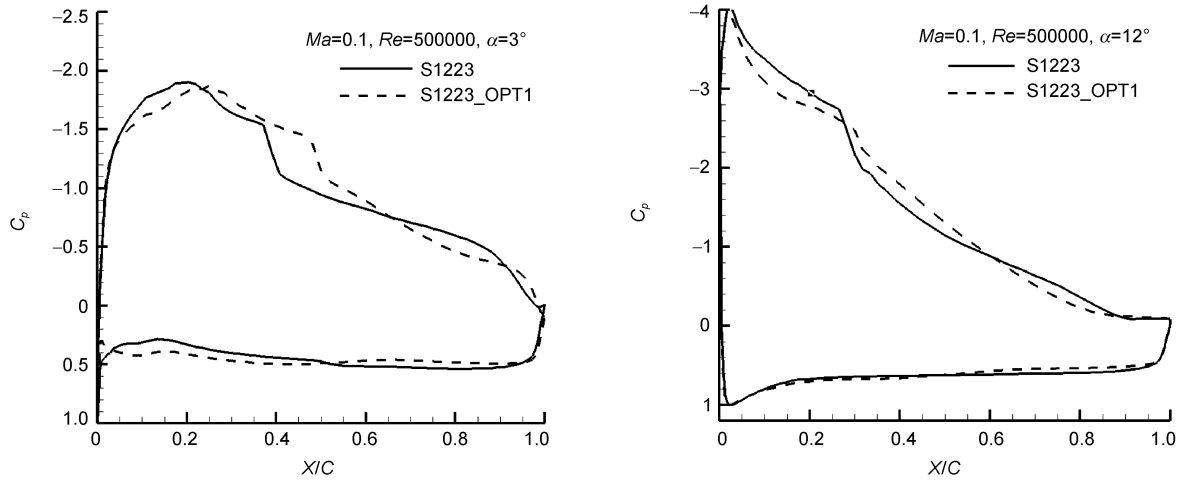

Figure 19 The surface static pressure distribution comparison between S1223 and S1223_OPT1.

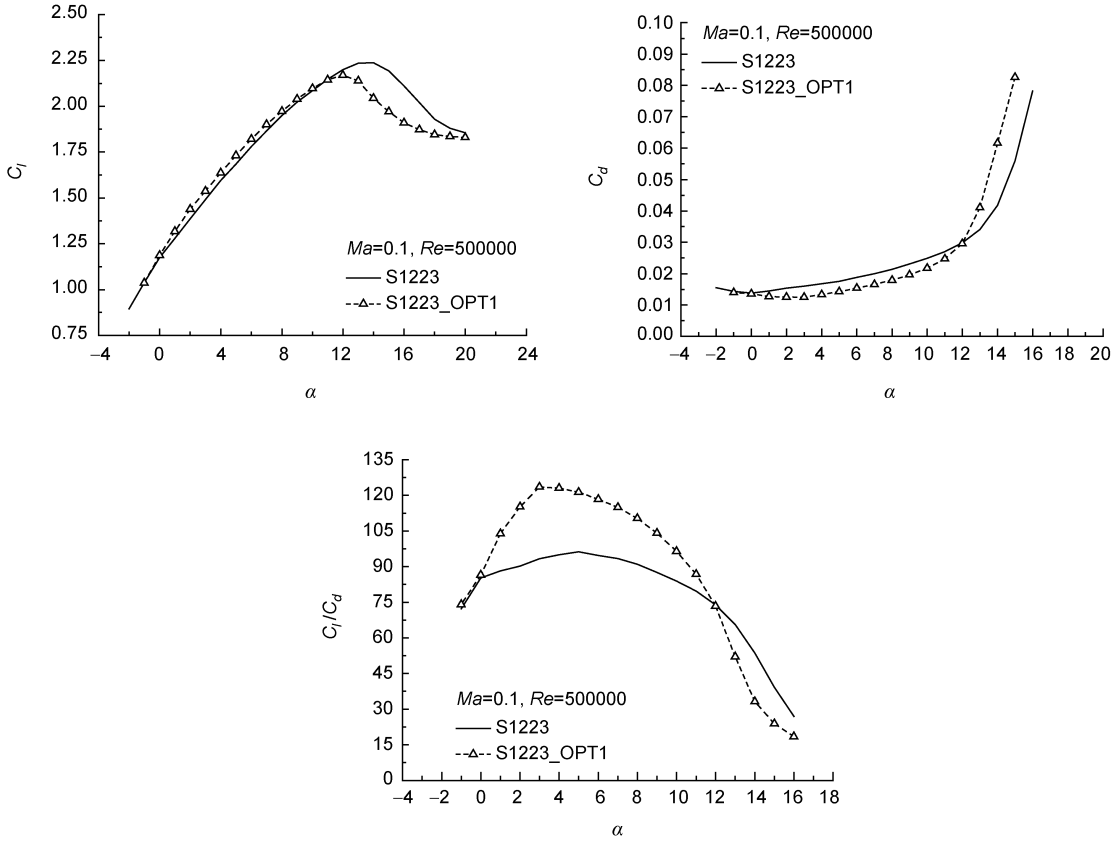

Figure 20 Aerodynamic computation comparison between S1223 and of S1223_OPT1.

Table 5 Results comparison between S1223 and S1223_OPT1 at the design attack angle α=3°

	C_l	ΔC_l	C_d	ΔC_d	C_l/C_d	$\Delta(C_l/C_d)$
S1223_3°	1.49		0.016		93.344	
S1223_OPT1_3°	1.5374	8.34%	0.0125	–21.9%	123.508	32.3%

1) $(C_d)_{\text{S1223\_OPT2}} \leqslant (C_d)_{\text{S1223}}$ at the primary design attack angle α=12°;

2) $(C_l)_{\text{S1223\_OPT2}} \geqslant (C_l)_{\text{S1223}}$ at the secondary design attack angle α=3°.

The optimized airfoil of the multi-objective optimization is described as S1223_OPT2 airfoil. Calculation data comparison between S1223 and S1223_OPT2 at the primary design attack angle α=12° and the secondary design attack angle α=3° are shown in Table 6. The comparisons of the contours and surface static pressure distributions among S1223, S1223_OPT1 and S1223_OPT2 are shown in Figures 21 and 22.

Figure 23 presents that the aerodynamic character of S1223_OPT2 is significantly better than those of S1223 and S1223_OPT1. From Table 6, it can be clearly seen that E387_OPT2 has a good aerodynamic performance at α=3° and 12°. The lift-coefficient of S1223_OPT2 declines from 2.20 to 2.37 at the primary design attack angle α=12°, a increase of 7.73%, along with an decreasing drag-coefficient of 15% (reaching 2.255), compared with S1223, which is obviously better than S1223_OPT1 at off-design attack angles $\alpha \geqslant$12°. At the same time, the drag-coefficient reduce from 0.016 to 0.0145 at the secondary design attack angle α=3°, an decrease of 9.4%, compared with S1223, along with the increasing lift coefficient of 8.34% (reaching 1.6143) and the increasing lift-drag ratio of 19.27% (reaching 111.33). At the same time, it can seen that S1223_OPT2 has a wide range of low drag.

As will be readily seen, the multiple design-points multi-objective optimization example for S1223 airfoil produces a satisfactory result. So the bi-objective optimization example presented here is resultful.

4 Conclusion

The high-performace low-Reynolds-number airfoil plays a decisive role for the success or failure of the propeller design of low-dynamic aircraft in stratosphere. To solve multi-point design problem of low-speed low-Reynolds-number airfoils, the paper demonstrates the hierarchical multi-objective optimization platform which combines the calculation of flow solver XFOIL with the direct search EXTREM optimization algorithm, based on analytic function linear superposition method used for establishing the shape of airfoils. From the optimization design results of design examples above, it can be clearly seen that the optimized airfoils E387_OPT2, FX63-137_OPT2 and S1223_OPT2 on the basis of low-Reynolds-number high-lift airfoils including E387, FX63-137 and S1223 can sufficiently meet

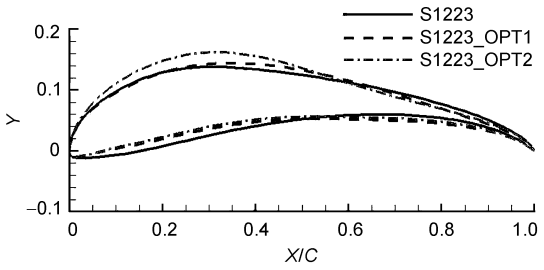

Figure 21 Contours among S1223, S1223_OPT1and S1223_OPT2.

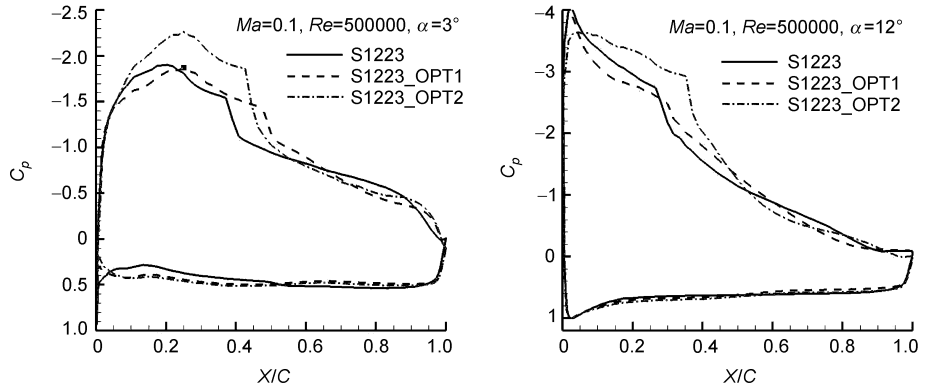

Figure 22 The surface static pressure distribution comparison among S1223, S1223_OPT1 and S1223_OPT2.

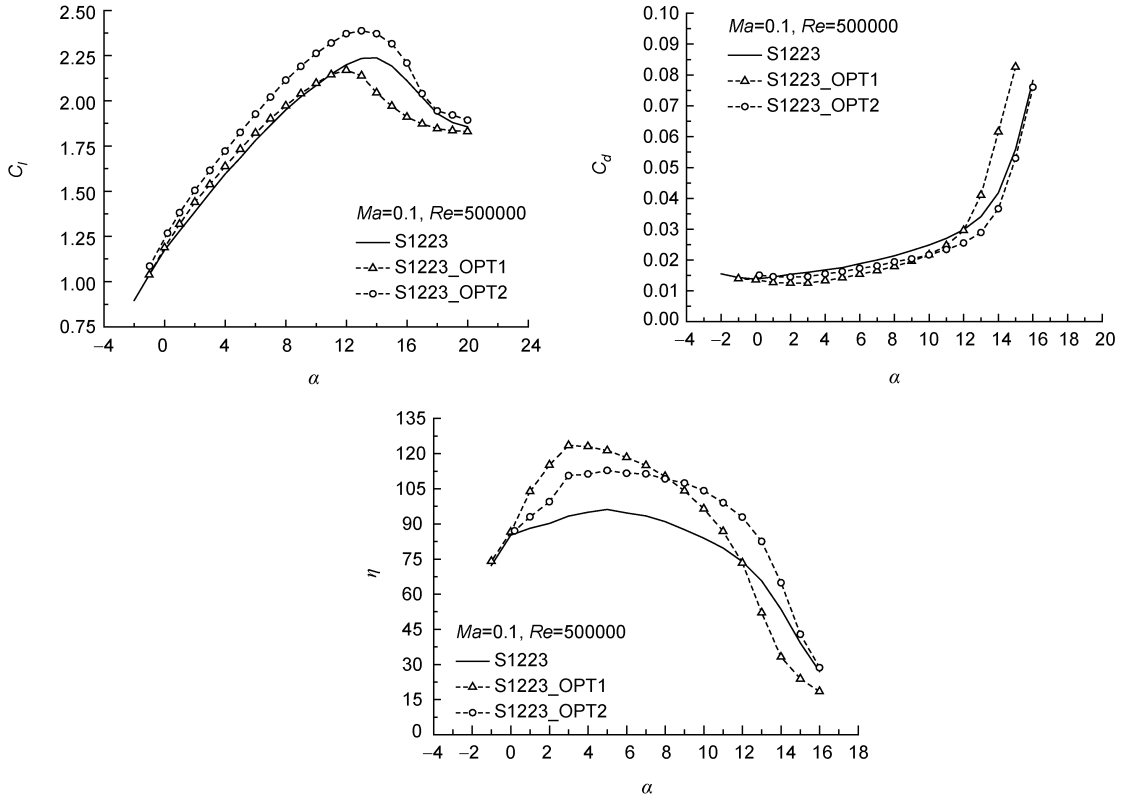

Figure 23 Aerodynamic computation comparison among S1223, S1223_OPT1 and S1223_OPT2.

Table 6 Results comparison between E387 and E387_OPT2 at multiple design-points

	C_l	ΔC_l	C_d	ΔC_d	C_l/C_d	$\Delta(C_l/C_d)$
S1223_12°	2.20		0.030		73.87	
S1223_OPT2_12°	2.37	7.73%	0.0255	–15%	92.85	25.7%
S1223_3°	1.49		0.016		93.344	
S1223_OPT2_3°	1.6143	8.34%	0.0145	–9.4%	111.33	19.27%

the optimization design requirements, which have good aerodynamic characteristics at the design and off-design conditions. Thus, the hierarchical multi-objective optimization platform presented here is effective for aerodynamics optimization design of a high-performance low Reynolds number airfoil for the propeller of low-dynamic vehicles in stratosphere.

This work was supported by the National Basic Research Program of China ("973" Project) (Grant No. 2009CB72400101) and the National Hi-Tech Research and Development Program of China ("863" Project) (Grant No. 2007AA705103).

1 Lewis J, Geoffrey S S, Isaac R. Porche III. High-altitude airships for the future force army. Technical Report (TR-234), 2005
2 Hao P F. The Future Stratospheric Airships. Beijing: Chinese Newlore Magazine, 2006. 12
3 Marcus Y, Stephanie K. An overview of advanced concepts for near-space systems. AIAA-2009-4805, 2009
4 Anthony C, Geoffrey A L. Long duration solar flight on venus. AIAA-2005-7156, 2005
5 Mueller T J. The influence of laminar separation and transition on low Reynolds number airfoil hysteresis. J Aircraft, 1985, 22: 764–770
6 Michael S S, James J G, Andy P B. Experiments on airfoils at low Reynolds number. AIAA-1996-62, 1996
7 Bai P, Cui E J, Li F, et al. Symmetrical airfoil low Reynolds number of small attack angle lift coefficients nonlinear phenomena research. Chin J Theor Appl Mech, 2006, 38: 1–8
8 Zhu Z Q, Wang X L, Wu Z C. Aerodynamic characteristics of small/micro unmanned aerial vehicles and their shape design. ACTA Aeronautica ET Astronautica Sinica, 2006, 27: 353–364
9 Donald G, Phil H. Design and predictions for high-altitude (low Reynolds number) aerodynamic flight experiment. NASA/TM-1999-206579, 1999
10 Liu Z, Zhu Z Q, Fu H Y, et al. Design for the high lift-drag ratio. In: The 12th Chinese National Computational Fluid Dynamics Conference, Taiwan, 2005
11 Fang B R. Design of Aircraft Aerodynamic Configuration. Beijing: Chinese Aviation Industry Press, 1997
12 Jacob H G. Rechnergesutzte Optimierung Statischer and Dyna-

mischer System. New York: Springer Verlag, 1982
13 Drela. XFOIL: an analysis and designing system for low Reynolds number airfoils. In: Low Reynolds Number Aerodynamics Proceedings of the Conference in Notre Dame. New York: Springer Verlag, 1989
14 XFOIL subsonic airfoil development system user guide. http://web.mit.edu/drela/Public/web/xfoil
15 Wang X P. Genetic algorithms and its application in the aerodynamic optimization design (in Chinese). Dissertation of Doctoral Degree. Xi'an: Northwest Polytechnical University, 2000
16 Hicks R, Henne P. Wing design by numerical optimization. J Aircraft, 1978, 15: 407–413
17 Zhong B W, Qiao Z D. Multiobjective optimization design of transonic airfoils. ICAS-94-2.1.1, 1994
18 Chris C C, Harry H H, Robert W B. Aerodynamic characteristics of NACA0012 airfoil section at angles of attack from 0 to 180°. National Advisory for Aeronautics Technical Note 3361, 1995
19 Thibert J J, Grandjacques M, Ohman L H. Experimental data base for computer program assessment. AGARD-AR-138, 1979
20 McGhee R J, Walker B S, Millard B F. Experimental results for the Eppler 387 airfoil at low Reynolds numbers in the Langley low-turbulence pressure tunnel. NASA TM-4062, 1988
21 Evangelista R, Pfenninger W, Mangalam S M, et al. Design and wind tunnel test of a high performance low Reynolds number airfoil. AIAA 87-2349, 1987
22 Selig M S, Guglielmo J J. High-lift low Reynolds number airfoil design. J Aircraft, 1997, 34: 10–15